渦法によるディフユーザポンプ非設計点の動静翼干渉の数値シミュレーション

Simulation of Unsteady Rotor-Stator Interaction at Off-design Points in a Diffuser Pump Using Advanced Vortex Method

祝　宝山　亀本　喬司
横浜国立大学　〒240-8501　横浜市保土ヶ谷区常盤台 79-5　zhu@post.me.ynu.ac.jp
Baoshan ZHU and Kyoji KAMEMOTO
Yokohama National University, 79-5 Tokiwadai, Hodogaya-ku, Yokohama, Japan

The interaction between impeller blades and diffuser vanes in a diffuser pump has been numerically simulated by using a direct vortex method for off-design operating conditions. Biot-Savart law was used to calculate velocity without the necessity to grid large portions of the flow field and the calculation points are concentrated in the regions where vorticity is present. Lagrangian representation of the evolving vorticity field is employed because it is suited to the moving boundaries. The pressure distribution was estimated directly from the instantaneous velocity and vorticity field with an integral pressure equation. The analysis of the simulation results and the comparison of calculation results with experimental ones show the method used in this paper is a fit tool to simulated the unsteady rotor-stator interaction in turbomachines.

1. Introduction

Unsteady rotor-stator interaction is very important for the design and operation of the turbomachines. Due to practical importance and the inherent complexity of the interaction phenomena, a large number of detailed experimental investigations and theoretical or numerical studies have reported in the literature regarding this problem. As measured and discussed by Dring et al.[1], the phenomenology of the rotor-stator dynamic interaction takes place mainly through two distinct mechanisms: potential and viscous interactions.

The potential flow effect is induced by the interaction of cascades in relative motion. These effects extend in both upstream and downstream directions. The rate of decay of potential perturbation is fast and hence the associated effect appears significant only in the case of small gaps between rotor and stator.

The viscous wake effect originates from the impingement and convection of the wakes shed from the preceding blades in the relative motion. When the impeller operates at off-design points, the flow separation occurs and separation bubbles are formed on the suction side or pressure side of the impeller blades for partial or exceeding discharge cases. With the impeller revolution, the vortex bubbles move downstream with the impeller blade wakes. Therefore, when a centrifugal impeller is combined with its vaned diffuser and operates at off-designed conditions, effects of the impeller on the diffuser will become more complicated and the viscous effects come from the impeller wakes as well as the passage vortices generated by impeller blades.

Numerical simulations of rotor-stator interactions in centrifugal turbomachines are complicated. The difficulties in simulating rotor-stator interaction are mainly due to two aspects: one is the grid connectivity from the rotary impeller to stationary diffuser, the other is the turbulent model. The applicability of turbulent models in the separation calculation is debated due to the effects of centrifugal force and Coriolis force on the flow field in the impeller. Qin & Tsukamoto[2] studied the unsteady flow in a diffuser pump analytically using the singularity method. Daws[3] simulated the unsteady interaction of a centrifugal impeller with its vaned diffuser using a k~ε turbulent model and a sliding surface to act as a transport internal boundary between the rotating and stationary frames.

Vortex methods have several merits, which may make them particularly well suited for simulations of high-Reynolds number flows. The vortex method based on the Biot-Savart law is a simple vortex method, which reduces the need to grid large portions of the flow field and concentrates the calculation points in the regions where vorticity is present. Lagrangian representation of the vorticity movement is well suited to moving boundaries. Utilizing the advantages of the vortex methods, an advanced scheme has been devised to simulate the unsteady impeller-diffuser interaction in a diffuser pump[4] for the designed operation. In the present paper, unsteady flow analysis will be extended to impeller-diffuser interaction at off-design points for the same diffuser pump.

2. Numerical Methods

2.1 Governing Equations

The two-dimensional incompressible unsteady flow of a viscous fluid may be determined by the vorticity transport equation as

$$\frac{\partial w}{\partial t} + \mathbf{v} \cdot \nabla w = n \nabla^2 w \quad , \tag{1}$$

where the vorticity is defined as

$$w = \nabla \times \mathbf{v} \quad . \tag{2}$$

Equations (1) and (2) are the governing equations of the vortex methods. Using the definition of vorticity and continuity $(\nabla \cdot \mathbf{v} = 0)$, it can be shown that $\mathbf{v}$ is related to w by the following Poisson equation:

$$\nabla^2 \mathbf{v} = -\nabla \times w \ . \tag{3}$$

This equation shows that the velocity field can be determined by the vorticity field.

2.2 Vortex Method

The present numerical method is based on the discretization of the above equations in a Lagrangian form using vortex methods. Velocity field is determined by the following Biot-Savart law,

$$\mathbf{v} = \frac{1}{2p}\int_V \frac{w \times \mathbf{R}}{R^2} dV + \frac{1}{2p}\int_S [\frac{(\mathbf{n}\cdot\mathbf{v})\cdot\mathbf{R}}{R^2} - \frac{(\mathbf{n}\times\mathbf{v})\times\mathbf{R}}{R^2}] dS \tag{4}$$

where $\mathbf{R}=\mathbf{r}-\mathbf{r}_0$, $\mathbf{R}=|\mathrm{R}|$, subscript $[_0]$ denotes a variable, differential or integral at location $\mathbf{r}_0$, $\mathbf{r}$ is an arbitrary location in the flow field. The first term in the right side represents the velocity induced by the vorticity existing in the flow field and the second term contains the contribution from the solid-body movement and the infinity velocity. The use of equation (4) to compute the velocity field guarantees the satisfaction of the boundary condition at infinity.

On the other hand, the vorticity transport equation (1) can be expressed in a Lagrangian formulation. Each discrete vortex follows the flow like a particle so the motion of fluid particles is presented by a single differential equation:

$$\frac{d\mathbf{r}}{dt} = \mathbf{v} \ . \tag{5}$$

For the calculation, the second-order Adams-Bashforth method was used to approximately compute the trajectory of the vortices. Another expression of the vorticity equation can be given in the following Lagrangian form.

$$\frac{dw}{dt} = n\nabla^2 w \tag{6}$$

The core-spreading method was utilized to consider effects of viscosity on the discrete vortices in the calculation.

Vorticity field near the solid surface must be correctly represented by proper distributions of vorticity layers and discrete vortex elements in order to satisfy the no-slip and no-flux conditions on the boundary surface. Details of the procedure used to simulate the vorticity transport, development and separation of the boundary layer near a solid boundary in this paper are described by Zhu[5]. For two-dimensional flow, the nascent vortices shed from the boundary are transformed into discrete rectangular elements with definite dimensions and uniform vorticity using this procedure. When these rectangular vortices move farther than a certain distance from the boundary surface, vortex blobs are used to replace the rectangular vortices. Conversely, vortex blobs may approach the boundary surface and may even penetrate the wall layer. In this method, their shape was retrained even as the blobs drew near the boundary. However when they passed the boundary surface, we could simply delete them.

2.3 Calculation of the Pressure

From the Navier-Stokes equation, the following integral equation can be obtained,

$$\begin{aligned}\int_V H\nabla^2 G dV + \int_S H\nabla G \cdot n dS = \\ -\int_S \partial\mathbf{v}/\partial t \cdot \mathbf{n} G dS - u\int_S (\nabla G \times w)\cdot \mathbf{n} dS \\ -\int_V \nabla \mathrm{G}\cdot(\mathbf{v}\times w)\mathrm{dV},\end{aligned} \tag{7}$$

where H is the Bernoulli function and G is the fundamental solution of the scalar Laplace equation. The expressions for H and G are respectively

$$H = \frac{p}{r} + \frac{v^2}{2} \tag{8}$$

$$G = \frac{1}{2p}\ln(\frac{1}{R}) \tag{9}$$

When the surface pressure is computed according to equation (7), the left-hand side of the equation represents a matrix concerned with H. The right-hand side accounts for the motion of the body and the field vorticity. Solution of the above equation yields the Bernoulli function H. Velocity $\mathbf{v}$ is usually known, so the pressure p can be easily calculated. With the results of H on the surface, we can use equation (7) again to compute H for an arbitrary location in the flow field where $\mathbf{v}$ can be computed according to the Biot-Savart law.

2.4 Application to Turbomachinery

Equation (4) can be directly used to calculate the unsteady flow velocity field induced by the impeller-diffuser interaction (figure 1). For the flow field within the impeller, the relative velocity $\mathbf{w}$ is usually used to analyze the flow characteristics. We have the following velocity relationship among the absolute velocity $\mathbf{v}$, relative velocity $\mathbf{w}$ and rotary velocity $\mathbf{u}$:

$$\mathbf{v} = \mathbf{w} + \mathbf{u} \tag{10}$$

From equation (10), the following acceleration equation can be obtained.

$$\frac{\partial \mathbf{v}}{\partial t} = \frac{\partial \mathbf{w}}{\partial t} - \nabla(\mathbf{u}\cdot\mathbf{v}) + \mathbf{u}\times(\nabla\times\mathbf{v}) \tag{11}$$

When equation (7) is used to calculate the pressure of the flow field shown in figure 1, on the surface S_d of diffuser vanes and an infinite surface S_∞ the term $\partial\mathbf{v}/\partial t$ is 0, whereas on the surface S_i of impeller blades, we should use the equation (11) to express the term $\partial\mathbf{v}/\partial t$. With substitution of equation (11) into equation (7), equation (7) can be rewritten as

$$\begin{aligned}\int_V H'\nabla^2 G dV + \int_S H'\nabla G\cdot n dS = \\ -\int_S \partial\mathbf{w}/\partial t \cdot \mathbf{n} G dS - u\int_S (\nabla G\times w)\cdot\mathbf{n} dS \\ -\int_V \nabla \mathrm{G}\cdot(\mathbf{w}\times w)\mathrm{dV}\end{aligned} \tag{12}$$

Where

$$H' = H - \mathbf{u}\cdot\mathbf{v} \tag{13}$$

In equation (12), the relative velocity $\mathbf{w}$ is 0 on the surface S_i, and the absolute velocity $\mathbf{v}$ on S_d and S_∞, is 0. Consequently, if the location, strength and velocity of the discrete vortices existing in the flow field are calculated, the pressure distribution can be easily calculated for the whole flow field.

3. Problem Statement

The specifications of the pump are summarized in Table 1. According to Table 1, the gap between the diffuser and the volute casing is so large that the effects of the volute casing on the impeller-diffuser interaction is neglected and so the calculated model is simplified as shown in figure 1. Some representative stations are shown in figure 2 for a vaned diffuser passage. The calculation stations are the same with the measurement stations[2]. For

the calculation, 50 vortex panels were distributed along the boundary surface of each blade for the impeller and diffuser at a height $h=4(v_o D_2/\nu)^{0.5}$, here v_o is the radial velocity at the entrance of the impeller, D_2 is the outlet diameter of the impeller and u is the kinematic viscosity. The size of the time step was dt=T/150, where T is the period of impeller revolution. About 2~3 periods of impeller revolution are required to produce an acceptable solution[4].

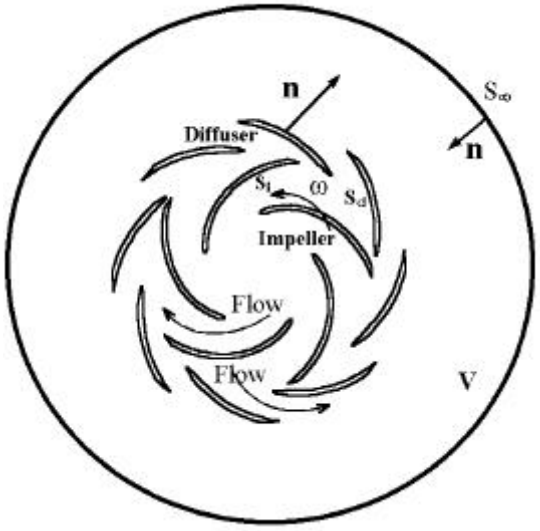

Figure 1 An impeller and its vaned diffuser

Table 1 Specifications of the test pump

Impeller:	Number of blades N_i=5
	Inlet diameter D_1=132.25 mm
	Outlet diameter D_2=250.00 mm
Diffuser:	Number of vanes N_d=8
	Inlet diameter D_3=258.00 mm
	Outlet diameter D_4=325.00 mm
Rating:	Flow rate Q_r=6.21 m^3/min
	Total headrise H_r=29.2 m
	Rotational speed $N = 2066$ rpm

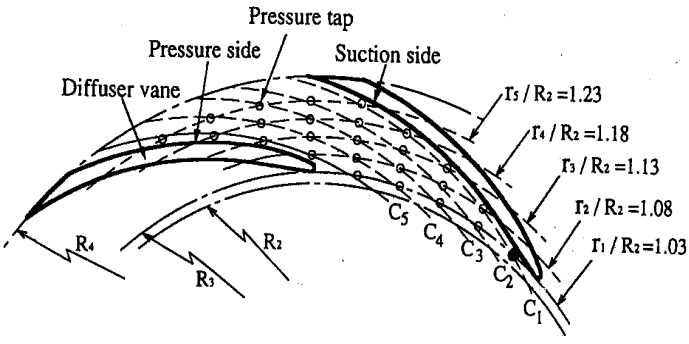

Figure 2 Representative stations for a passage in the diffuser

4. Results and Discussions

4.1 Unsteady Velocity Field

Besides the designed condition, we have also calculated the off-design operation conditions for Q/Q_r=0.4, 0.6, 0.8, and 1.2 . When the impeller operates at off-design points, separation will occur on the impeller blades with the flow impingement. The instantaneous vortex flow patterns for partial discharge case Q/Q_r=0.6, 1.0 and 1.2 are represented in figure 3, here T_i is the one-blade passing time. In figure 3, the blue points represent the discrete vortices with positive vorticity (counter-clockwise vorticity) and the red ones represent the discrete vortices with minus vorticity (clockwise vorticity). These figures represent the interaction of the inviscid flow field generated by the impeller and diffuser in relative motion and the transport of separation vortices with blade wakes from upstream impeller blades.

For partial discharge case Q/Q_r=0.6, in the suction side of the impeller blades, large-scale vortex bubbles are formed. On the other hand, for exceeding flow discharge Q/Q_r=1.2, the separation vortex bubbles are formed along the pressure side of the impeller blades. Both for Q/Q_r=0.6 and Q/Q_r=1.2, the differences in the size and shape of the separation bubbles can be found, which are possibly caused by the unsymmetry of the diffuser vanes to the impeller blades. With the impeller revolution, these strong vortices will be transferred into the diffuser with the blade wakes.

Therefore when a centrifugal impeller is combined with its vaned diffuser and operates at off-design points, effects of the impeller on the diffuser become more complicated and the viscous effects include the impeller wakes as well as the passage vortices generated by flow separation around the impeller blades. With time marching, these vortices will be decayed by fluid viscosity and turbulence. Effects of the differential connective velocity in the vane-to-vane passage are also clearly evident from the vortex traces. The vortices on the suction side of the diffuser vanes travel much faster than the vortices on the pressure side, being distorted and elongated.

4.2 Unsteady Pressure

Figure 4 shows the instantaneous static pressure distributions corresponding to the flow patterns shown in figure 3. Both for partial discharge case Q/Q_r=0.6 and exceeding discharge case Q/Q_r=1.2, pressure of the flow separation zones is very low in the impeller and the instantaneous pressure distribution is clearly unsymmetrical both in the impeller and diffuser. As the impeller rotates, significant variations occur in the static pressure at the diffuser inlet.

The dependence of the pressure fluctuations on the flow discharge in the diffuser is presented in figure 5. We show the pressure fluctuations at taps (r_1,c_3), (r_3,c_3) and (r_5,c_3) (figure 2) in figure 5. For each tap, the pressure increases as the discharge decreases. At the same time, as the discharge drifts off the designed point, with the occurrence of separation, the effects of the viscosity increase according to the fluctuations of unsteady pressure.

Figure 6 presents the distribution of the magnitude DC_p for unsteady pressure fluctuations at the diffuser inlet from (r_L,c_1) to (r_1,c_5) (figure 2) for different flow discharges, here DC_p is the peak-to-peak value of the unsteady pressure. Both calculated and measured results show the same tendency that the magnitude DC_p of unsteady pressure increases with the increasing flow

discharge Q in the case of Q/Q_r>0.8. The measured DC_p is the smallest near Q/Q_r=0.6 and it increases with decreasing flow discharge Q in the case of Q/Q_r<0.6. For the calculated results, DC_p is the smallest near Q/Q_r=0.8 and it increases with flow discharge decreasing in the case of Q/Q_r<0.8.

5. Conclusions

In this study, the unsteady interaction of a centrifugal impeller with its vaned diffuser has been investigated for the off-design operation conditions. The instantaneous flow patterns show that the whole flow characteristics induced by rotor-stator interaction operating at off-design conditions can be caught by using the vortex method of this paper. A quantitative agreement has been achieved in the unsteady pressure calculation for the diffuser inlet compared with the experimental results. Both calculated and measured pressures show that there is a flow discharge, at which the magnitude of unsteady pressure is the smallest.

The unsteady rotor-stator interaction in turbomachines is a complicated flow phenomenon, especially for off-design operations. The results of the present study confirm that the advanced vortex method used in this paper is applicable for investigating the unsteady interaction of a rotating impeller with a stationary diffuser in turbomachinery, even for the off-design operation conditions. In order to achieve the quantitative analyses through numerical simulation, the high-resolution vortex methods are needed to give much accurate results.

6. References

[1] Dring, P.R., Joslyn, H.W. and Wagner, J.H., Turbine Rotor-Stator Interaction, ASME Journal of Engineering for Power, Vol.104, (1982), pp.213-222.

[2] Qin, W. and Tsukamoto, H., Theoretical Study of Pressure Fluctuations Downstream of a Diffuser Pump Impeller -Part 1: Fundamental Analysis on Rotor-Stator Interaction, Part 2: Effects of Volute, Flow Rate and Radial Gap, ASME Journal of Fluids Engineering, Vol.119, (1997), pp.647-652 & pp.653-658.

[3] Daws, W.N., A Simulation of the unsteady Interaction of a Centrifugal Impeller with Its Vaned Diffuser: Flow Analysis, ASME Journal of Turbomachinery, Vol.117 (1995), pp.213-222.

[4] Zhu, B. and Kamemoto, K., Simulation of the Unsteady Interaction of a Centrifugal Impeller with its Diffuser by an Advanced Vortex Method, JSME International Journal Series B, Vol.43 (2000), No.3, pp.372-379.

[5] Zhu, B., Study on Application of an Advanced Vortex Method to Unsteady Flow Analysis in Tubomachinery, (1999), Doctoral Thesis, Yokohama National University, Japan.

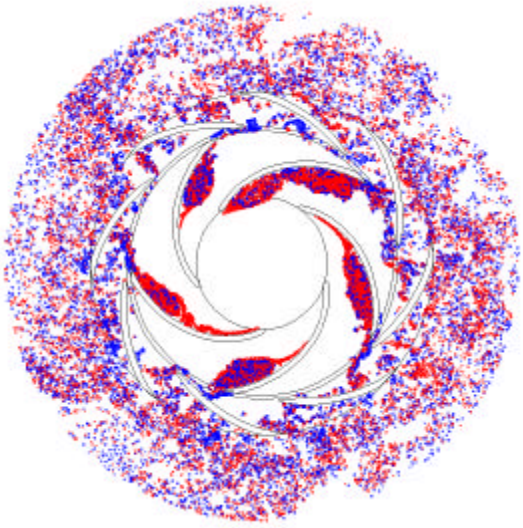

(1) $t/T_i=0$

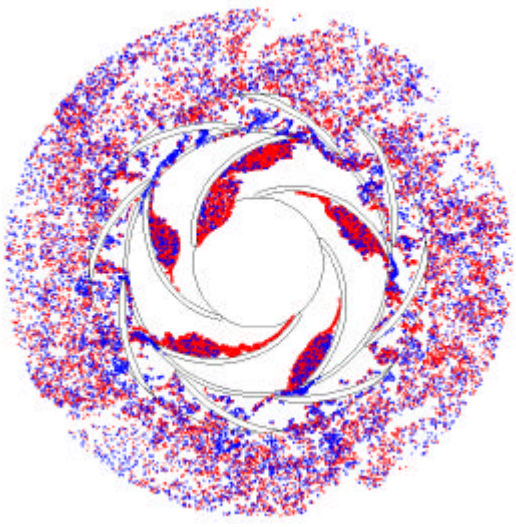

(2) $t/T_i=1/2$

(a) Partial discharge $Q/Q_r=0.6$

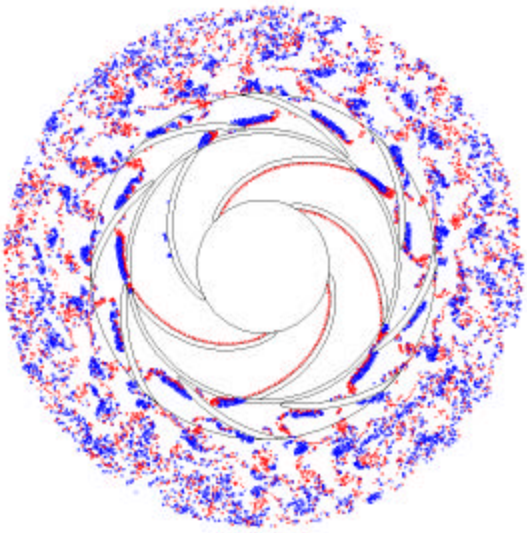

(1) $t/T_i=0$

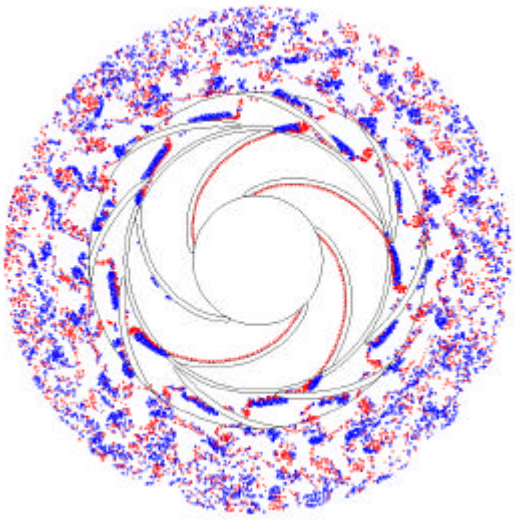

(2) $t/T_i=1/2$

(b) Design discharge $Q/Q_r=1.0$

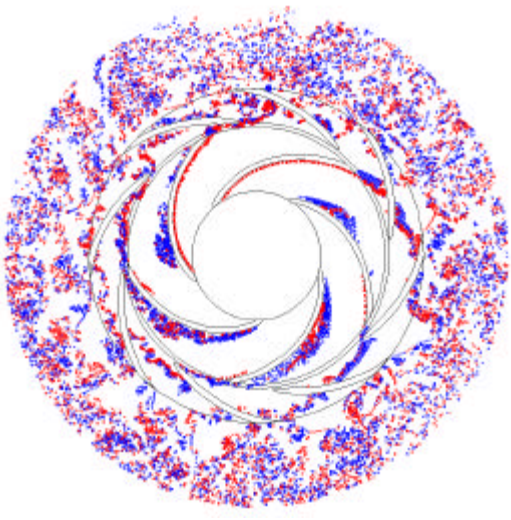

(1) $t/T_i=0$

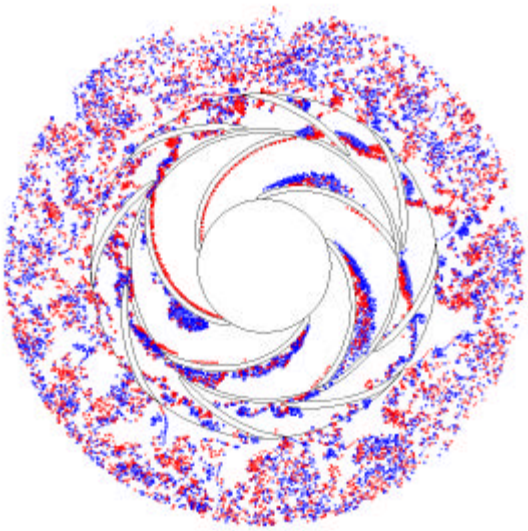

(2) $t/T_i=1/2$

(c) Exceeding discharge $Q/Q_r=1.2$

Figure 3 Flow patterns represented by discrete vortices

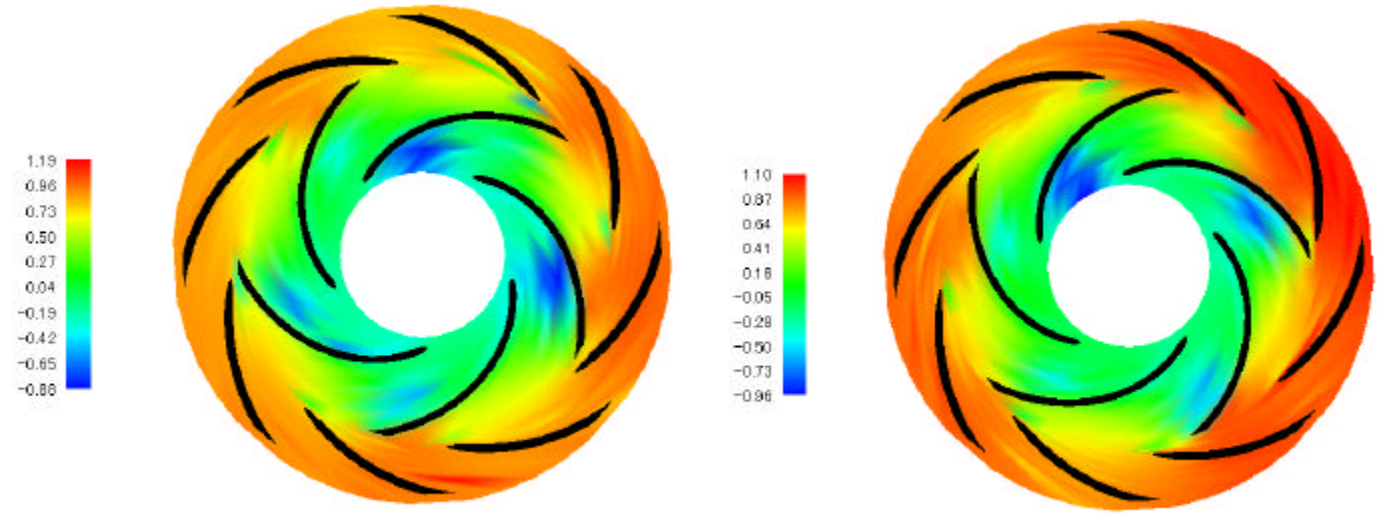

(1) $t/T_i=0$ (2) $t/T_i=1/2$

(a) Partial discharge $Q/Q_r=0.6$

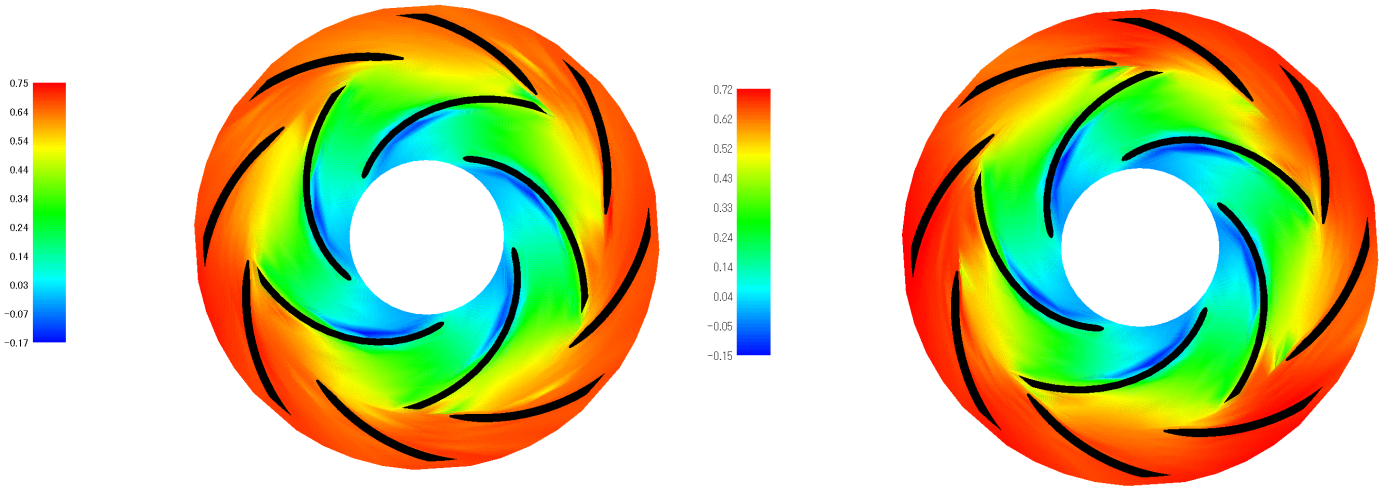

(1) $t/T_i=0$ (2) $t/T_i=1/2$

(b) Design discharge $Q/Q_r=1.0$

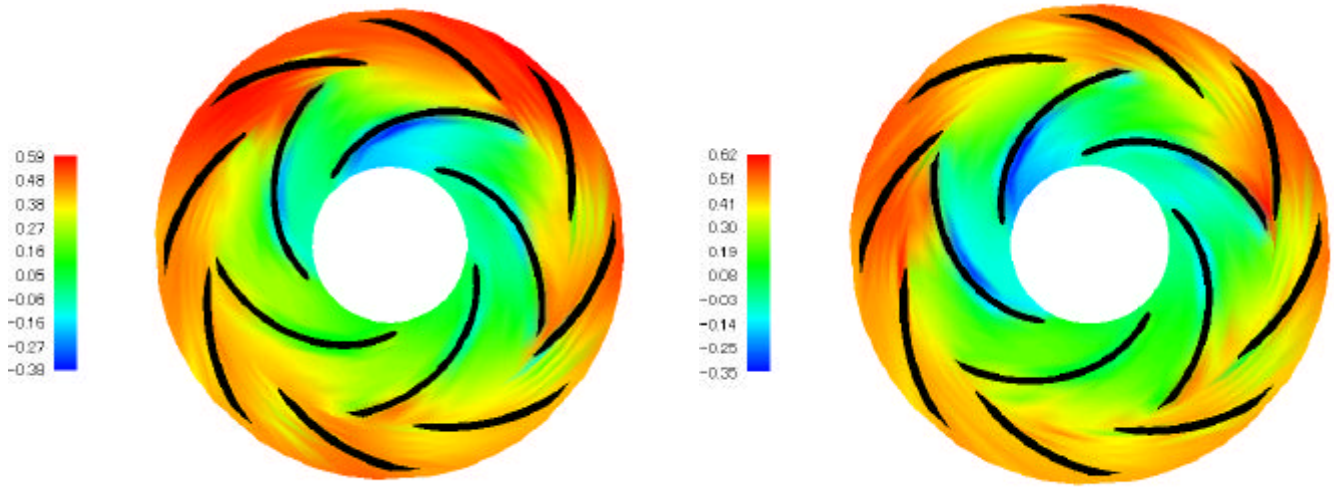

(1) $t/T_i=0$ (2) $t/T_i=1/2$

(c) Exceeding discharge $Q/Q_r=1.2$

Figure 4 Contours of static pressure

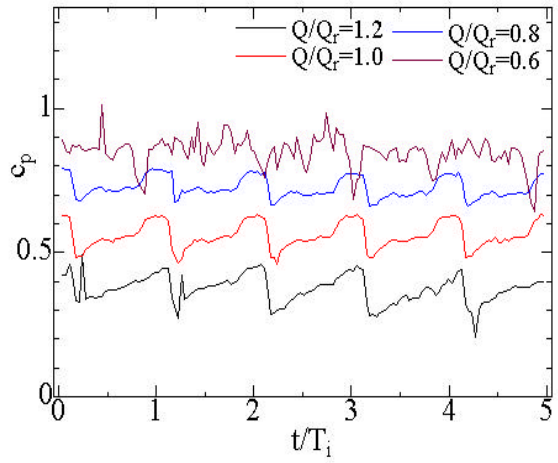

(a) (r_1,c_3)

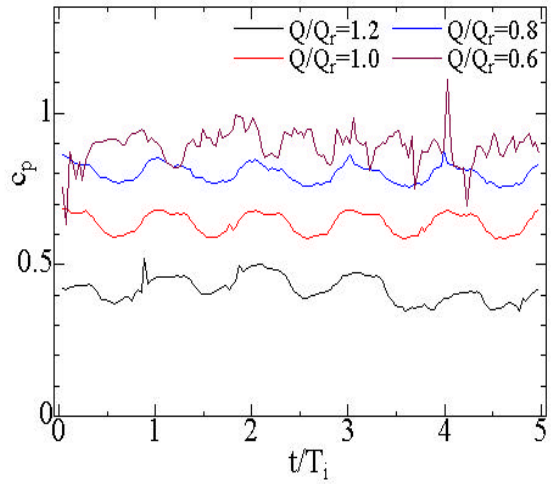

(b) (r_3,c_3)

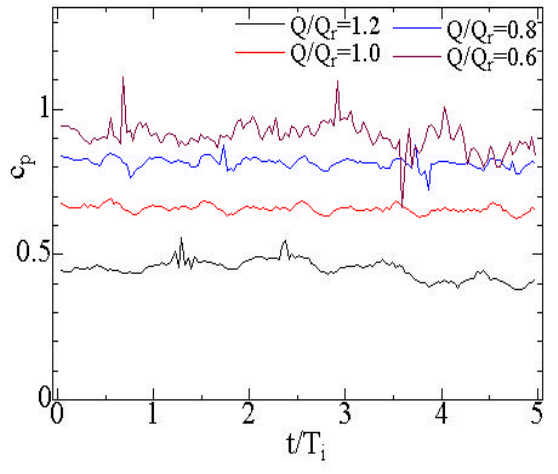

(c) (r_5,c_3)

Figure 5 Variation of the static pressure with time at some taps

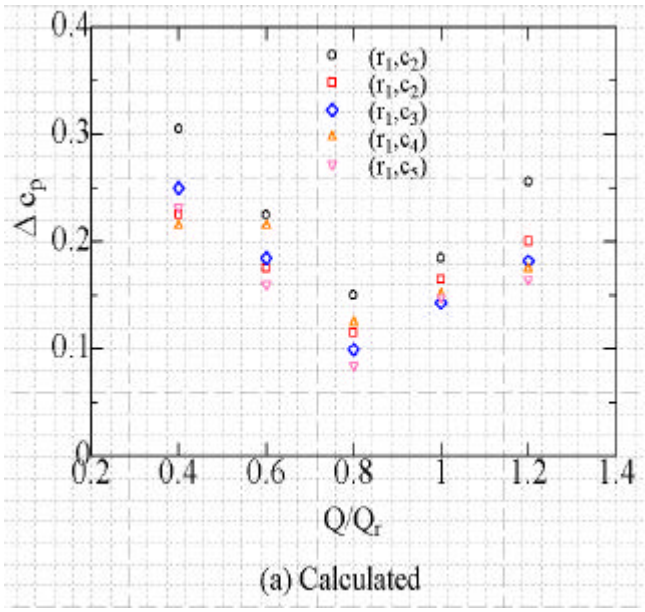

(a) Calculated

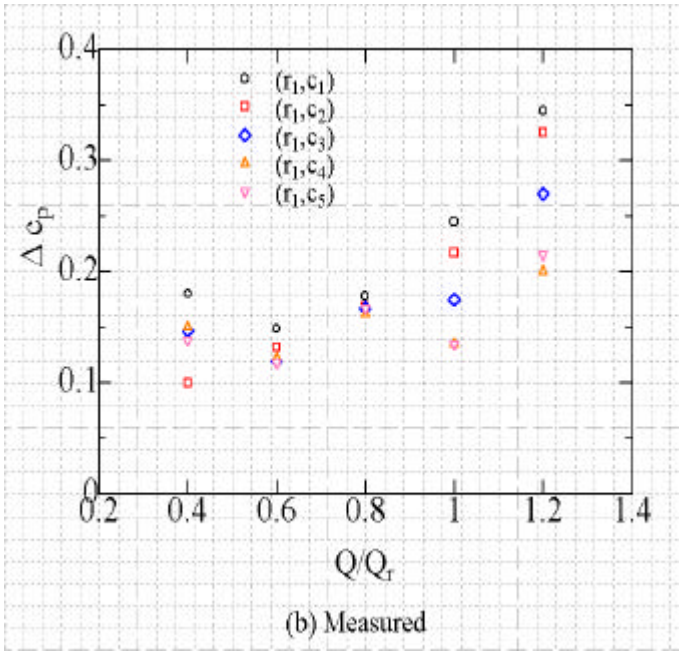

(b) Measured

Figure 6 Magnitude of the unsteady pressure at diffuser inlet